PERGAMON

International Journal of Heat and Mass Transfer 45 (2002) 2141–2152

International Journal of HEAT and MASS TRANSFER

www.elsevier.com/locate/ijhmt

Laminar natural convection in an inclined cavity with a wavy wall

L. Adjlout *, O. Imine, A. Azzi, M. Belkadi

Institut de Génie Maritime, USTO BP 1505 Oran ElMnaouer, Algeria

Received 22 March 1999; received in revised form 24 July 2001

Abstract

In the present work, a numerical study of the effect of a hot wavy wall of a laminar natural convection in an inclined square cavity, differentially heated, was carried out. This problem is solved by using the partial differential equations, which are the vorticity transport, heat transfer and stream function in curvilinear co-ordinates. The tests were performed for different inclination angles, amplitudes and Rayleigh numbers while the Prandtl number was kept constant. Two geometrical configurations were used namely one and three undulations.

The results obtained show that the hot wall undulation affects the flow and the heat transfer rate in the cavity. The mean Nusselt number decreases comparing with the square cavity. The trend of the local heat transfer is wavy. The frequency of the latter is different from the undulated wall frequency. © 2002 Published by Elsevier Science Ltd.

1. Introduction

The study of the natural convection in the cavities has been the focus on a lot of investigations during the last three decades because of the multiple applications in which it is involved. Many experimental and numerical studies have emphasised on the natural convection in the cavity. Since the work of Ostrach [1], Catton [2] and Yang [3] which have shown the importance of the inclined cavity, a more comprehension of the flow behaviour and the heat transfer in such cavities were needed. The study of the extreme cases such as the Benard problem and the cavity with the heated vertical walls, has shown the influence of the inclination angle on the flow characteristics [4]. Then, the different regimes of the flow have been studied for the inclined cavities as described in the work of Hollands and Konicek [5] and Hollands [6] in terms of the critical Rayleigh number related to the stability of the confined flow. The study of the aspect ratio and inclination angle influence has allowed the understanding of the Nusselt number evolution [7] and the finding of some correlation for the Nusselt number calculation [8,9].

The use of different boundary conditions has shown that the flow and the heat transfer are seriously affected [10–13]. This was also the case when the variable properties such as the thermal conductivity, the viscosity and the heat capacity are varied [14].

During the last few years, some interesting results on the natural convection for both laminar and turbulent flow in an inclined square cavity have been found by the authors in [15–17]. An extension work on the natural convection in inclined cavities has been performed. In [18,19], the influence of partitions in the geometry and changes in the geometry has been investigated.

On the other hand, Yao [20] has studied theoretically the natural convection along a vertical wavy surface. He found the heat transfer rate for a wavy surface was constantly smaller than that of corresponding flat plate. The influence of the geometrical parameters on the mean Nusselt number is clearly shown from his results. Adding to the latter, the amplitude, the wavelength and mainly the wave number should be taken into account. From the latter findings and for the geometry changes in the cavity, Adjlout et al. [21] have studied the influence of the undulation number in a rectangular cavity differentially heated with a vertical undulated hot wall on the heat transfer rate.

In the present paper, a numerical study of the influence of the wavy hot wall in an inclined square

* Corresponding author.
E-mail address: imine_b@altavista.com (L. Adjlout).

0017-9310/02/$ - see front matter © 2002 Published by Elsevier Science Ltd.
PII: S0017-9310(01)00304-0

Nomenclature

a	thermal diffusivity
g	gravitational acceleration
J	Jacobian of the transformation
$L^f F = [(f\eta F)\xi - (f\xi F)\eta]/J$	operator
$Nu_l = (y_\eta \cos\tau - x_\eta \sin\tau)(\mathrm{d}\theta/\mathrm{d}\xi)(1/J)$	Nu Nusselt number
$Pr = \nu/a$	Prandtl number
$Ra = \overline{\beta} g l^3 (T_h - T_c)/(a\nu)$	Rayleigh number
S	curvilinear coordinate on the wavy wall
T	temperature
u, v	velocity components on x and y
$\boldsymbol{U}$	velocity vector
x, y	Cartesian co-ordinates
Y	ordinate

Greek symbols

$\overline{\beta}$	thermal dilatation coefficient
$\beta = x\xi x\eta + y\xi y\eta$	transformation factor
$\alpha = x\eta x_\eta + y\eta y_\eta$	
$\gamma = x\xi x\xi + y\xi y\xi$	
ξ, η	co-ordinates of the transformed domain
ν	kinematic viscosity
ρ	density
ϕ	inclination angle
ψ	stream function
ω	vorticity
τ	angle between the normal to the wall and x-axis
$\partial/\partial n$	gradient normal
∇	operator nabla
∇^2	operator Laplace
$\bar{\nabla}^2 = [\alpha\partial_{\xi\xi} - 2/\beta\partial_{\xi\eta} + \gamma\partial_{\eta\eta} + J^2(P\partial_\eta + Q\partial_\xi)]/J^2$	

Indices

x, y, ξ, η, t	derivative relative to x, y, ξ, η and t
h,c	hot wall and cold wall

cavity on a laminar natural convection has been performed. A sinusoidal wall is chosen for the hot wall and different amplitudes of undulation were investigated. One and three undulations are presented in the present work. The fluid used is air. The present study will focus on the influence of the inclination angle on the local Nusselt number distribution for various Rayleigh numbers. Furthermore, stream line and isotherm study of the hydrodynamic and thermal boundary layers has been performed providing more details of the flow and the heat transfer near the wavy wall.

2. Analysis

The problem treated is a two-dimensional heat transfer in an inclined square cavity. The hot wall is wavy with a constant temperature T_h. The cold wall is opposite to the latter with a constant temperature T_c while the other sides are insulated. The Rayleigh number is varied up to 10^6 while Prandtl number is fixed to be 0.71. Fig. 1 shows the geometrical features of the cavity used.

The viscous incompressible flow inside a closed cavity and a temperature distribution is described by the Navier–Stokes and the energy equations. The Boussinesq approximation is used with the assumptions of constant properties and negligible viscous dissipation. The governing equations are defined as follows:

$$\frac{\partial^2\psi}{\partial x^2} + \frac{\partial^2\psi}{\partial y^2} = -\omega, \tag{1}$$

$$\frac{\partial\omega}{\partial t} + u\frac{\partial\omega}{\partial x} + v\frac{\partial\omega}{\partial y} = \mu\left(\frac{\partial^2\omega}{\partial x^2} + \frac{\partial^2\omega}{\partial y^2}\right) + \rho g\overline{\beta}\left(\sin\phi\frac{\partial T}{\partial y} + \cos\phi\frac{\partial T}{\partial x}\right), \tag{2}$$

$$\frac{\partial T}{\partial t} + u\frac{\partial T}{\partial x} + v\frac{\partial T}{\partial y} = a\left(\frac{\partial^2 T}{\partial x^2} + \frac{\partial^2 T}{\partial y^2}\right). \tag{3}$$

With the following boundary conditions

$$\begin{aligned} &T = T_h, \quad u = v = 0 \quad \text{on the hot wall,}\\ &T = T_c, \quad u = v = 0 \quad \text{on the cold wall,}\\ &\frac{\partial T}{\partial n} = 0, \quad u = v = 0 \quad \text{on the rest.} \end{aligned} \tag{4}$$

Hence, introducing the following non-dimensioned variables:

$$(x, y)^* = (x, y)/l,$$

$$(u, v)^* = (u, v)l/a,$$

$$\theta = (T - T_0)/(T_h - T_c) \quad \text{with } T_0 = (T_h + T_c)/2.$$

$$Pr = \nu/a,$$

$$Ra = \overline{\beta} g l^3 (T_h - T_c)/(a\nu). \tag{5}$$

The equations of the problem are now expressed as follows:

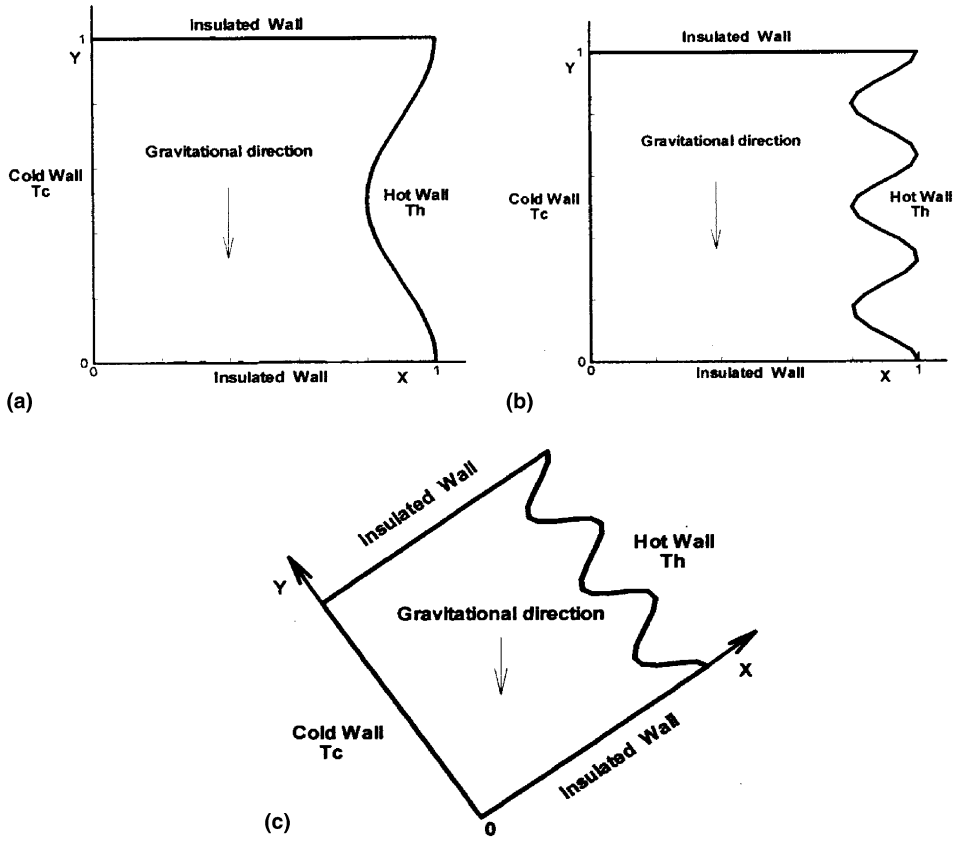

Fig. 1. Geometrical feautures of the used cavity: (a) one undulation; (b) three undulations; (c) inclined cavity.

$$\frac{\partial^2\psi}{\partial x^2}+\frac{\partial^2\psi}{\partial y^2}=-\omega, \tag{6}$$

$$\frac{\partial\omega}{\partial t}+u\frac{\partial\omega}{\partial x}+v\frac{\partial\omega}{\partial y}=Pr\left(\frac{\partial^2\omega}{\partial x^2}+\frac{\partial^2\omega}{\partial y^2}\right)+PrRa\left(\sin\phi\frac{\partial\theta}{\partial y}+\cos\phi\frac{\partial\theta}{\partial x}\right), \tag{7}$$

$$\frac{\partial\theta}{\partial t}+u\frac{\partial\theta}{\partial x}+v\frac{\partial\theta}{\partial y}=a\left(\frac{\partial^2\theta}{\partial x^2}+\frac{\partial^2\theta}{\partial y^2}\right). \tag{8}$$

The study is completed with the definition of the following boundary conditions:

$$\begin{aligned}&\theta=-0.5,\quad u=v=0 \qquad \text{on the cold wall},\\ &\theta=0.5,\quad u=v=0 \qquad \text{on the hot wall},\\ &\theta_n=0,\quad u=v=0 \qquad \text{on the rest.}\end{aligned} \tag{9}$$

3. Numerical procedure

The grid generation calculation is based on the curvilinear co-ordinate system applied to fluid flow as described by Thompson et al. [22]. The transformation is as follows:

$$\xi=\xi(x,y),\quad \eta=\eta(x,y) \quad \text{for } 0\leqslant\xi\leqslant1,\ 0\leqslant\eta\leqslant1. \tag{10}$$

Knowing that

$$0\leqslant y\leqslant1$$

and

$$0\leqslant x\leqslant f(y)$$

with

$$f(y)=[1-\mathrm{Amp}+\mathrm{Amp}(\cos 2\pi ny)],\quad \eta=y,\ \ x=x(\xi,\eta), \tag{11}$$

where n and Amp are, respectively, a number of undulation and amplitude.

The problem is now defined in terms of new variables:

$$L^{\psi}\omega=Pr\widetilde{\nabla}^2\omega+RaPr(\cos\phi L^{y}\theta-\sin\phi L^{x}\theta), \tag{12}$$

$$\widetilde{\nabla}^2\psi=-\omega, \tag{13}$$

$$L^{\psi}\theta = \widetilde{\nabla}^2\theta, \tag{14}$$

where the operators $L^{\psi}\omega, L^{x}\theta, L^{y}\theta$ and $\widetilde{\nabla}^2$ are defined in the nomenclature, and the following boundary conditions are:

$$\xi = 0, \quad \psi = 0, \quad \theta = -0.5, \quad \omega = -\frac{\alpha}{J^2}\psi_{\xi\xi},$$

$$\xi = 1, \quad \psi = 0, \quad \theta = 0.5, \quad \omega = -\frac{\alpha}{J^2}\psi_{\xi\xi},$$

$$\eta = 0, \quad \psi = 0, \quad \theta_{\eta} = 0, \quad \omega = -\frac{\gamma}{J^2}\psi_{\eta\eta},$$

$$\eta = 1, \quad \psi = 0, \quad \theta_{\eta} = 0, \quad \omega = -\frac{\gamma}{J^2}\psi_{\eta\eta}, \tag{15}$$

The boundary conditions for the vorticity are obtained from Eq. (15) and the stream function value on the walls.

The heat transfer rate by convection in an enclosure is obtained from the Nusselt number calculation. On the wavy wall, the local Nusselt number is expressed as:

$$Nu_{\mathrm{l}} = (y_{\eta}\cos\tau - x_{\eta}\sin\tau)\frac{\mathrm{d}\theta}{\mathrm{d}\xi}\frac{1}{J}. \tag{16}$$

While the mean Nusselt number is the average of the local Nusselt number along the wavy wall and is defined by the following equation:

$$Nu_{\mathrm{a}} = \frac{1}{s}\int_0^s \left((y_{\eta}\cos\tau - x_{\eta}\sin\tau)\frac{\mathrm{d}\theta}{\mathrm{d}\xi}\frac{1}{J}\right)\mathrm{d}s. \tag{17}$$

The governing equations are discretised by a finite difference method. The resolution of the equation system is performed by an implicit method with an alternate difference implicit (ADI) scheme. This scheme leads to the tridiagonal matrix obtained from a semi-iterative line by line procedure. The simplified Gauss elimination method is used to solve this system. The marching step is used for the vorticity resolution. The non-linearity and strong coupling of the equations needs an under relaxation to ensure convergence. The relaxation factors are used for stream function, vorticity and temperature equations and are, respectively, 1.0, 0.2 and 0.5.

Different grids were used namely $(31 \times 31), (42 \times 42)$ and (50×50). The calculations were performed on Pentium II, 128 Mo RAM. Typical run to reach steady state for (42×42) grid takes about 3 min CPU time.

4. Results

Several grids have been tested for the case of $Ra = 10^5$, $\phi = 90°$ and the amplitude of 0.05. Table 1 shows the average Nusselt number for the three grids used, at $Ra = 10^5, \phi = 90°$ and the amplitude of undulation 0.05.

Table 1
Comparison on Nusselt number at several grids for $Ra = 10^5, \phi = 90°$ and the amplitude 0.05

	31×31	42×42	50×50
One undulation	3.65	3.68	3.71
Three undulations	3.52	3.51	3.53

It is clearly seen that there is a little difference between the three grid results and the grid of (42×42) is used in all subsequent calculations.

The discussion of the following results concerns the temperature and streamline distributions, the heat transfer rate and the local Nusselt number for the undulated cavities at different inclination angles (0°, 30°, 60°, 90°, 120°, 150°, and 180°). The results were for Rayleigh of 10^5 and the undulation amplitude of 0.05. In Figs. 2–5 the direction of the gravity is indicated by the arrows.

4.1. Cavity with one undulation, $Ra = 10^5$

The angular position $\phi = 0°$ corresponds to the Benard problem, where it is clearly seen the presence of two counter-rotating rolls disposed on both sides of the symmetrical axis of the cavity, even with the low fluid motion as shown in Fig. 2(a). In the median part, the fluid hits the undulation crest resulting in a heat transfer increase in this region. The latter is confirmed with the isotherm distribution near the hot wall as shown in Fig. 3(a). These isotherm lines pass near the crest then move away from the wall trough. It is shown in the same figure that in the remaining part of the cavity the heat transfer is purely conductive. The local Nusselt number distribution on the hot wall shows a slight increase of this number near the crest, which vanishes when approaching the wall trough (Fig. 6).

When the angle ϕ is increased to 30°, the gravitation component perpendicular to the adiabatic walls is present. A fluid motion is starting along the wall cavity resulting in a change of position of the two cells parallel to the symmetrical axis as shown in Fig. 2(b). The thermoconvective movement causes an isotherm line deviation (Fig. 3(b)). In the central part of the cavity, the isotherms stay perpendicular to the gravitation. In the neighbourhood of the hot wall, the thermal boundary layer thickness increases in the flow direction. This remark is confirmed with the local Nusselt number distribution shown in Fig. 6. However, the heat transfer by diffusion remains dominant.

At the angle of $\phi = 60°$, there is a shrink of the two rolls in the perpendicular direction to the symmetrical axis of the cavity as shown in Fig. 2(c). The flow is accelerated just after the bottom corner of the hot wall and near the top corner of the normal wall. This gives a big

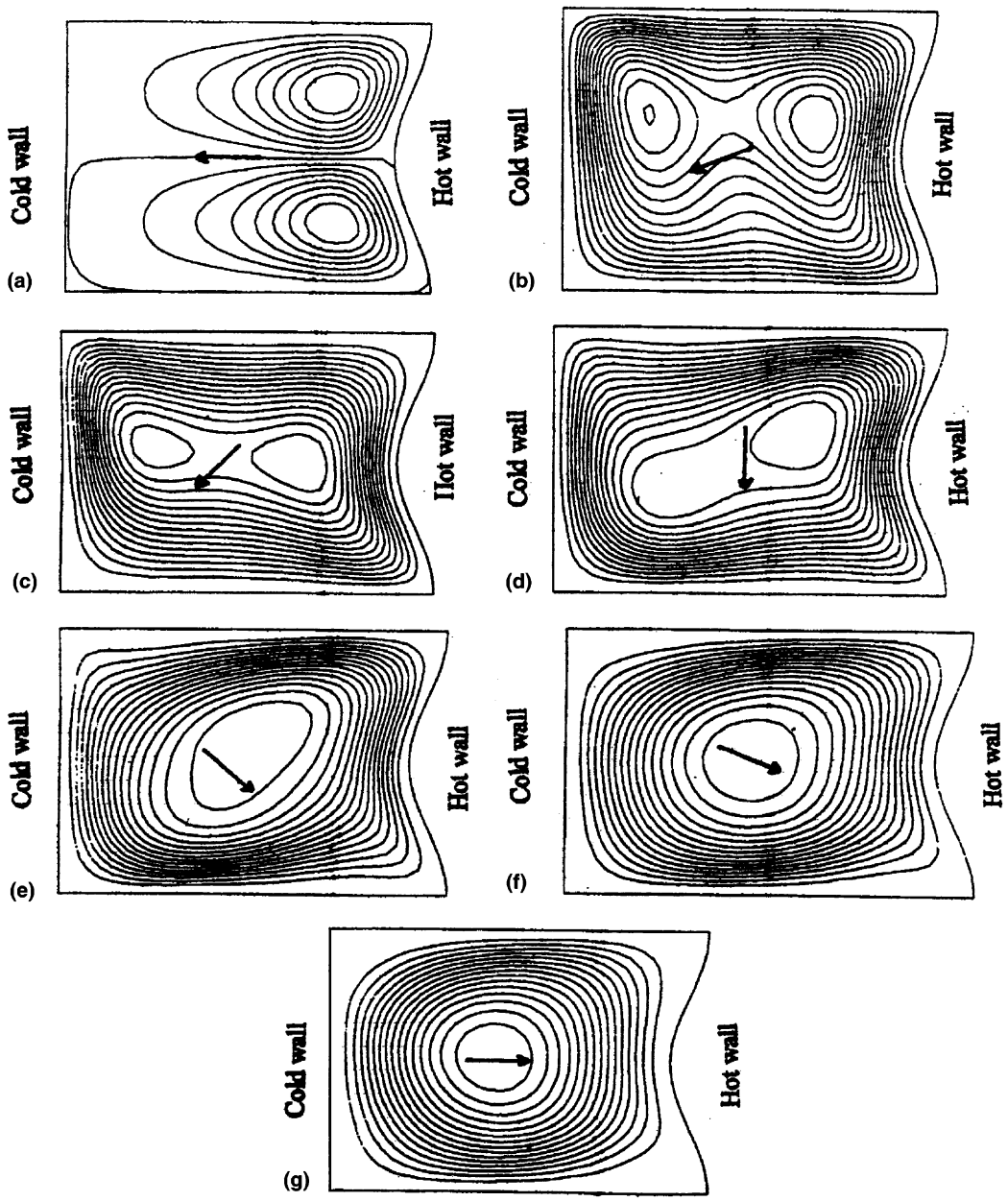

Fig. 2. Streamline distributions for different angles and Rayleigh of 10^5: (a) streamline distribution for angle 0°; (b) streamline distribution for angle 30°; (c) streamline distribution for angle 60°; (d) streamline distribution for angle 90°; (e) streamline distribution for angle 120°; (f) streamline distribution for angle 150°; (g) streamline distribution for angle 180°.

increase of the heat transfer caused by the fact that the fluid in these regions hits, respectively, the hot and cold walls. The local Nusselt number, as shown in Fig. 6, is indeed high in these zones. The isotherm lines in the central region of the cavity stay perpendicular to the gravitation giving a stratification situation of the fluid in this zone (Fig. 3(c)). The thermal boundary layer is growing along the isotherm walls. However, near the crest, the isotherm lines stay quasi-parallel to the wall. This situation is also observed for the streamlines near the crest. The effect caused by the latter is explained by the presence of an almost horizontal inflection near the crest in the local Nusselt number distribution as shown in Fig. 6.

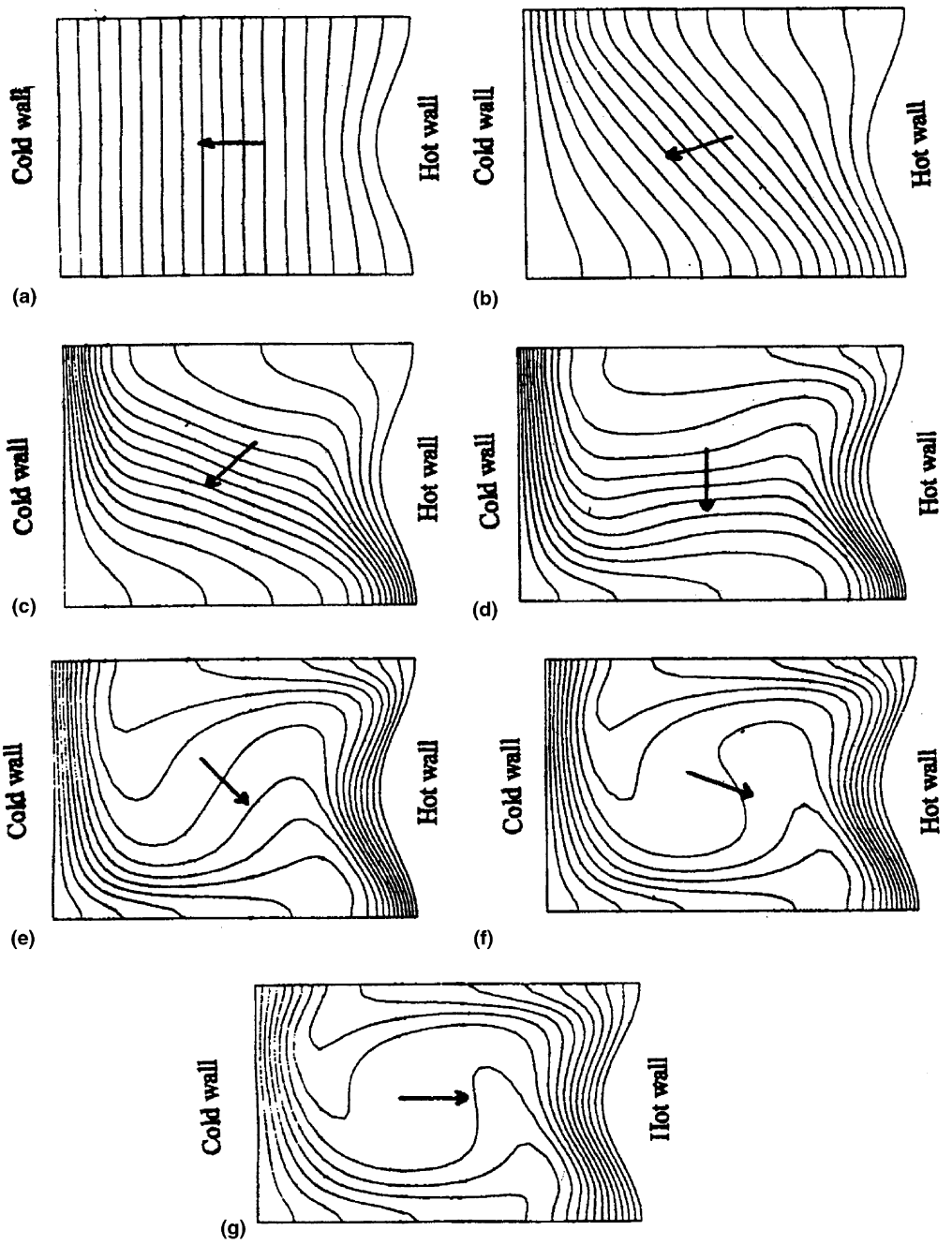

Fig. 3. Temperature distributions for different angles and Rayleigh of 10^5: (a) temperature distribution for angle 0°; (b) temperature distribution for angle 30°; (c) temperature distribution for angle 60°; (d) temperature distribution for angle 90°; (e) temperature distribution for angle 120°; (f) temperature distribution for angle 150°; (g) temperature distribution for angle 180°.

At the angle of $\phi = 90°$, the gravitation is perpendicular to the adiabatic walls. Fig. 2(d) shows the thermoconvective flow accelerating more and is represented by the form of one diagonally stretched cell. Near the crest, the streamlines move near the wall just after the crest. The isotherm distribution shows the same feature near the latter region as presented by Fig. 3(d). This observation proves the diminution of the thermal

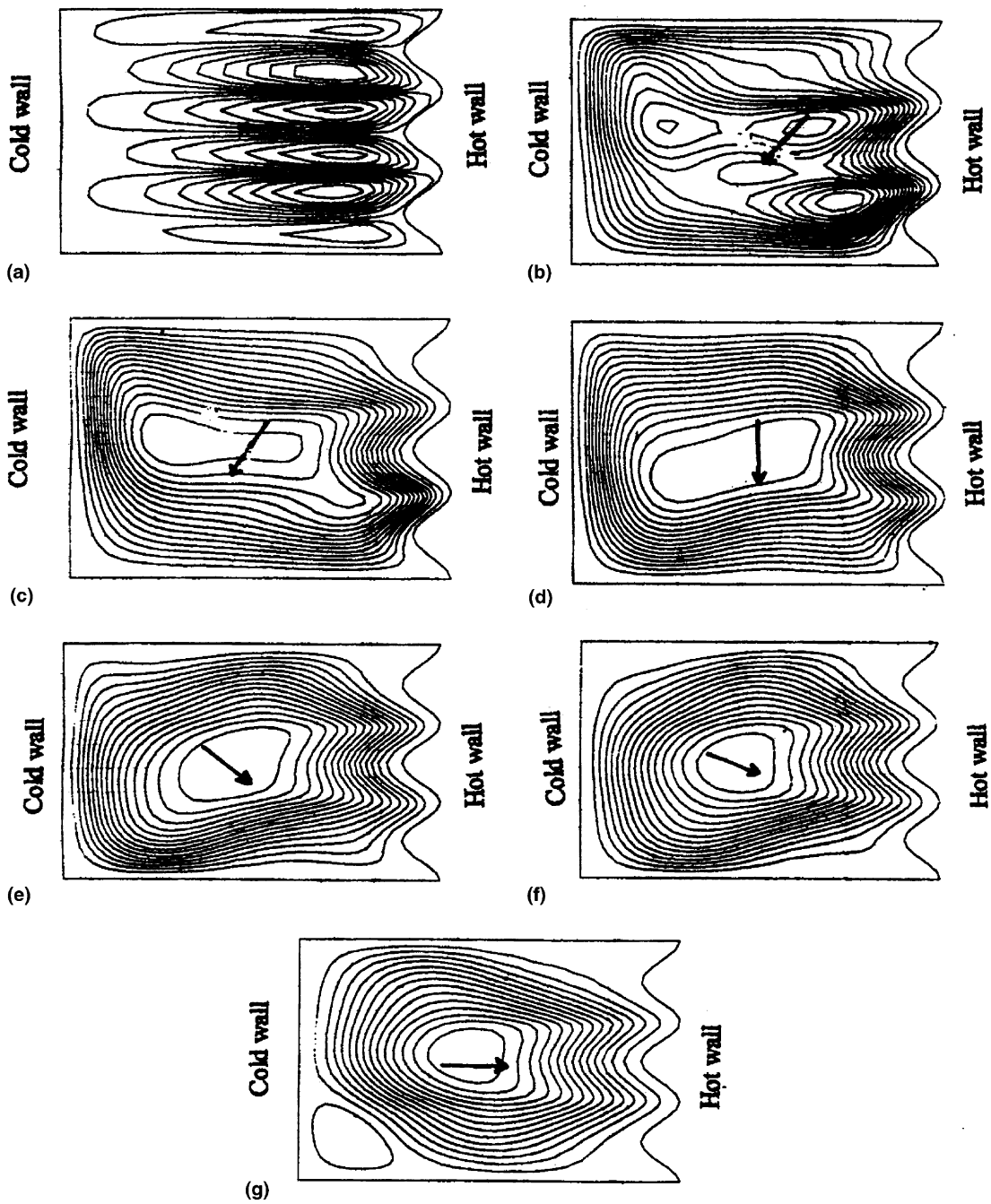

Fig. 4. Streamline distributions for different angles and Rayleigh of 10^5: (a) streamline distribution for angle 0°; (b) streamline distribution for angle 30°; (c) streamline distribution for angle 60°; (d) streamline distribution for angle 90°; (e) streamline distribution for angle 120°; (f) streamline distribution for angle 150°; (g) streamline distribution for angle 180°.

boundary layer thickness just after the crest. The local Nusselt number distribution confirms this finding while the latter variation is the inverted of the thermal boundary layer thickness as seen in Fig. 6. The flow stays stratified in the core region of the cavity.

At the angle of $\phi = 120°$ and $\phi = 150°$, the flow is monocellular as shown in Figs. 2(e) and (f). The temperature distributions are shown in Figs. 3(e) and (f). Near and along the hot wall, the boundary layer thickness increases then decreases under the effect of the

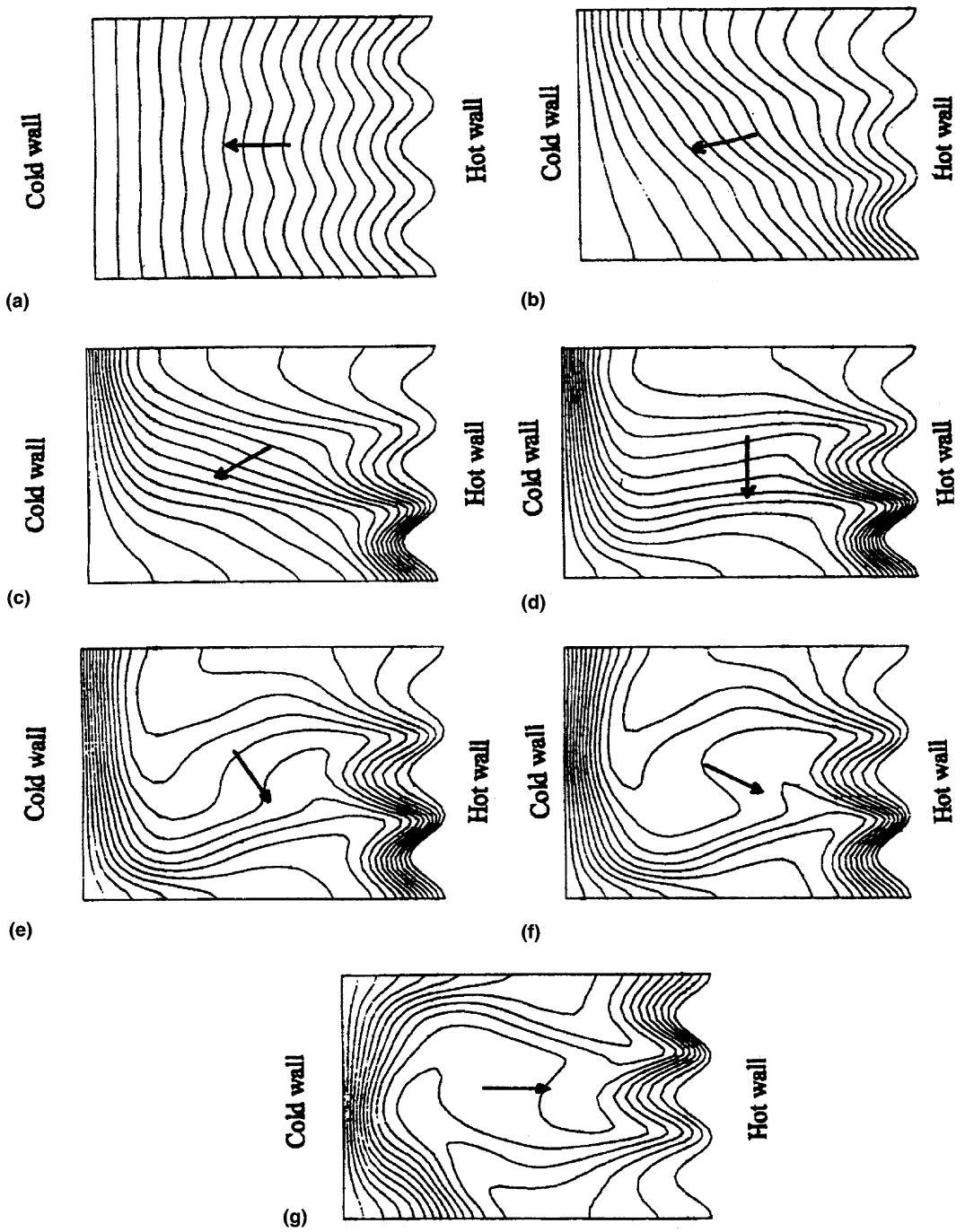

Fig. 5. Temperature distributions for different angles and Rayleigh of 10^5: (a) temperature distribution for angle 0°; (b) temperature distribution for angle 30°; (c) temperature distribution for angle 60°; (d) temperature distribution for angle 90°; (e) temperature distribution for angle 120°; (f) temperature distribution for angle 150°; (g) temperature distribution for angle 180°.

undulation. Consequently, the local Nusselt number decreases in the crest zone and increases before it as observed in Fig. 6. The isotherm lines near the isotherm walls are more dense for the case of $\phi = 120°$ than for $\phi = 150°$. This shows that the heat transfer diminishes for ϕ greater than 120°.

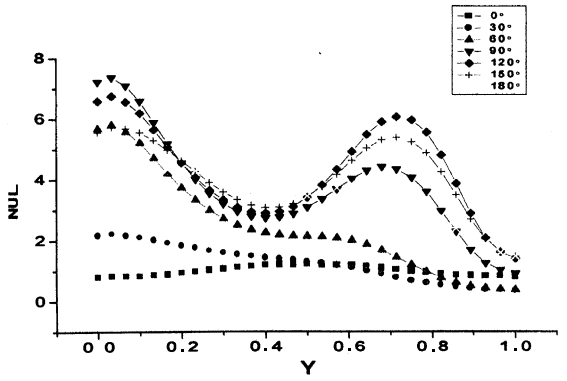

Fig. 6. Local Nusselt number distributions for one undulation and for $Ra = 10^5$.

The calculations for $\phi = 180°$ have converged proving that the undulated cavity delays more the limits of the tridimensional flow which is present in the case.

Fig. 2(g) shows that the flow stays under the form of one quasi-circular cell. The trend of the isotherm lines is not different from the above one as shown in Fig. 3(g). The heat transfer decreases more near the isotherm walls. The trend of the local Nusselt number distribution makes in evidence the persistence of the undulation influence as presented in Fig. 6.

4.2. Cavity with three undulation, $Ra = 10^5$

The streamline distributions inside the cavity with three undulations for the respective angle $\phi = 0°$, 30°, 60°, 90°, 120°, 150° and 180° are presented in Fig. 4.

At $\phi = 0°$, six Benard rolls appear in the cavity. However, their movement is so low that the heat transfer mode is purely conductive as shown in Figs. 5(a) and 7.

Apart from the cases of $\phi = 30°$ and $\phi = 180°$, the flow in the cavity is monocellular as exhibited in Figs. 4(c)–(f). It is clear that the undulated wall has an influence on the geometrical form taken by the cell as it is noticed on the different streamline patterns. In particular, near the hot wall, the streamlines converge toward the wall after each crest and diverge after each trough. This behaviour has a repercussion on the heat transfer by convection near the wall. Indeed, when the normal velocity component approaches the streamline to the wall, the heat transfer increases. The examination of the isotherm lines and the local Nusselt number distribution as described by Figs. 5(b)–(f) and Fig. 7 reveals that the thermal boundary layer thickness on the side of the undulated wall increases and decreases just before a crest or just after a trough. The local Nusselt number peaks move forward with an increase of the inclination angle.

For the case of $\phi = 180°$, near the cell dominating the major part of the cavity surface, appears a corner cell in the opposite direction of the main one and hence decreases the heat transfer by convection (Figs. 4(g), 5(g) and 7). The local Nusselt number peaks have moved clearly comparing with the precedent cases. This is probably due to the important rotation velocity in the present case.

It is clearly seen, after examination of Figs. 6 and 7, that the heat transfer is maximum for the configuration of $\phi = 90°$.

4.3. Local Nusselt number comparison

Fig. 8 represents a comparison between the local Nusselt number distributions for one and three undulations with the results of the square cavities from [23,24] for an angle of $\phi = 90°$. The undulated feature of the local Nusselt is well established for the wavy wall cavity as observed in the latter figure. The undulation frequency of Nusselt distribution is slightly different from the undulated wall frequency. Indeed, for the configuration with one undulation, the frequency is higher than the wall frequency, while it is lower than for the configuration with three undulations. It has to be

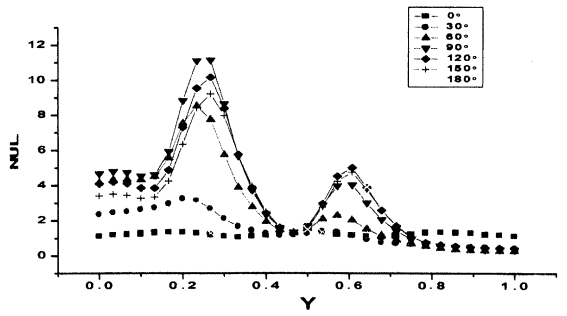

Fig. 7. Local Nusselt number for three undulation and for $Ra = 10^5$.

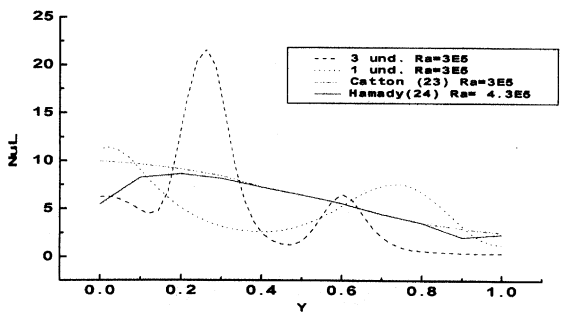

Fig. 8. Comparison of local Nusselt number results for $\phi = 90°$.

noted that Yao [20] has found for the vertical wavy plate a frequency twice that of the wall. The mean variation of these distributions follows the same trend as for the square cavity but the difference between them is notable.

4.4. Averaged Nusselt number

The comparison of the averaged Nusselt number function of Rayleigh number between the undulated cavities and the squares cavities [14,24] for an angle of $\phi = 90°$ is presented in Fig. 9. This comparison is for a Rayleigh number up to 10^6. The influence of the wall undulations is clearly seen in the latter figure by a clear decrease in Nusselt number comparing with the square cavities. The difference between the averaged Nusselt number of [14] and the cavity with three undulations increases with an increase in the Rayleigh number. On the other hand, the configuration with one undulation has a mean Nusselt number higher than the configuration with three undulations.

Fig. 10 shows the averaged Nusselt number against the inclination angle for a Rayleigh number of 10^5. For the square cavity, the curve presented here, is obtained by the formulae of [14] and is expressed as follows:

$$Nu_a = (Nu_a(90°) - Nu_a(0°)) \times (2/\pi) \times (\phi \sin(\phi)) + Nu_a(0°) \quad \text{for } \phi \leqslant 150°,$$
$$Nu_a = Nu_a(180°) \times (\cos(\phi - 180°)) \quad \text{for } \phi > 150°. \tag{18}$$

The averaged Nusselt number remains low for the undulated cavities in the range 0–180° exception for the neighbourhood of the inclination angle of 150° where the configuration with one undulation manifests an averaged Nusselt number very slightly higher than the one for the square cavity. This figure also shows that the minimum of the averaged Nusselt number is obtained for an angle of $\phi = 180°$ which is in agreement with the results of Ozoe et al. [13].

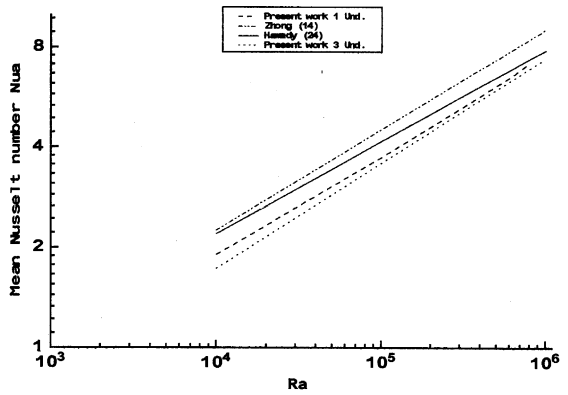

Fig. 9. Comparison of the mean Nusselt number results for $\phi = 90°$.

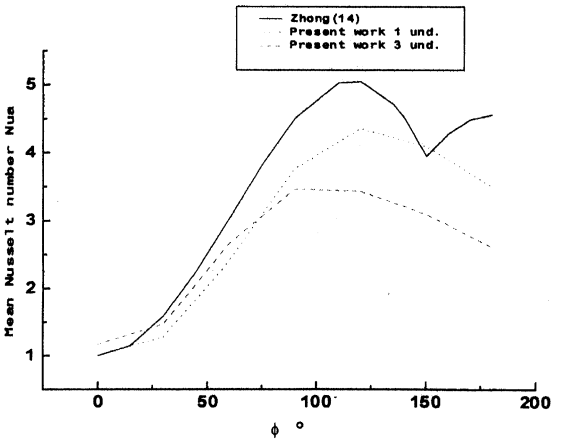

Fig. 10. Comparison of the mean Nusselt number at $Ra = 10^5$.

The three undulated configuration has an averaged Nusselt number slightly higher than the cavity with one undulation up to 75°, over this value, the opposite occurs and the difference increases with an increase in the inclination angle.

4.5. Influence of the amplitude of the undulation

The distributions of local Nusselt number for different amplitudes for three undulations at $Ra = 10^5$ are shown in Fig. 11. The same trend is observed for the four tested amplitudes. There is a decrease of the local Nusselt number on the whole wall with an increase in the amplitude of the undulation.

The comparison on the mean Nusselt number for different amplitudes of undulation was performed for the case of one and three undulations and it is shown in Table 2.

It is noted that the mean Nusselt number decreases with an increase in the amplitude of the undulation. This result has also been found by Yao [20]. The undulated wall leads to an increase of the heat exchange area as

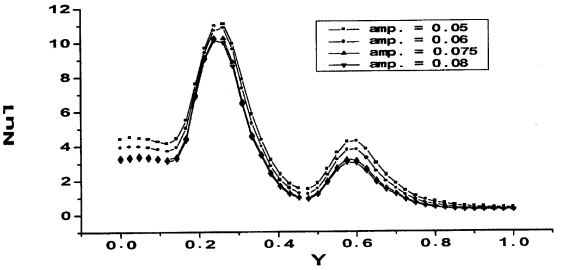

Fig. 11. Local Nusselt number for three undulation and for $Ra = 10^5$.

Table 2
Mean Nusselt number and length of undulation at $Ra = 10^5$ for different amplitudes

Amplitude	0.05	0.06	0.075	0.08
Nu_a for one undulation	3.68	3.57	3.43	3.38
Nu_a for three undulations	3.51	3.24	2.89	2.80
Length of one undulation	1.02	1.03	1.05	1.06
Length of three undulations	1.18	1.25	1.37	1.41

shown in Table 2. However, for the case of one undulation, the relative decrease of the mean Nusselt number (11.3%, 13.5%, 17.5% and 18.5%) comparing with a square cavity [24] is higher than the increase in the area of the undulated wall, respectively (2%, 3%, 5% and 6%). On the other hand, for the case of three undulations, the increase of the heat exchange area (18%, 25%, 37% and 41%) is slightly higher than the average Nusselt number, respectively (15.4%, 21.5%, 30.6% and 32.5%). In both cases, a heat transfer by convection slightly decreases. Furthermore, in a solar collectors for example, the exchange by radiation increases with the increase of the exchange area.

5. Conclusion

The present work deals with the effect of the undulated hot wall on the heat transfer by natural convection in an inclined square cavity, heated differentially. The study is performed numerically for a laminar free convection. The results obtained for different inclination angles and for different Rayleigh numbers show that the flow and the heat transfer are affected by the undulation of the hot wall. Indeed, the latter acts on the thermal boundary layer that thickened or thinned along this wall. Consequently, an undulated feature is given to the local Nusselt number distribution resulting in a decrease of the heat transfer rate comparing with the square cavity. It seems also that an increase in the undulation number on the hot wall reduces the heat transfer rate for an inclination angle greater than 75°.

Acknowledgements

The authors wish to give special thanks for Prof. A Mir of Ecole Superieure de Technologie d'Agadir, Prof. Jamoule and Dhang of Mechanical Department of Liege University.

References

[1] S. Ostrach, Natural convection in enclosures, in: J.P. Hartnett, T.F. Irvine Jr. (Eds.), Advances in Heat Transfer, vol. 8, Academic Press, New York, 1972, pp. 161–227.

[2] I. Catton, Natural convection in enclosures, in: Proceedings of the Sixth International Heat Transfer Conference, vol. 6, 1978, pp. 13–31.

[3] K.T. Yang, Transitions and bifurcations in laminar buoyant flows in confined enclosures, J. Heat Transfer 110 (1988) 1191–1204.

[4] J.E. Hart, Stability of the flow in a differentially heated inclined box, J. Fluid Mech. 47 (1991) 547–576.

[5] K.G.T. Hollands, L. Konicek, Experimental study of the stability of differentially heated inclined air layers, Int. J. Heat Mass Transfer 16 (1973) 1467–1476.

[6] K.G.T. Hollands, Natural convection in horizontal thin-walled honeycomb panels, J. Heat Transfer 95 (1973) 439–444.

[7] J.N. Arnold, I. Catton, D.K. Edwards, Experimental investigation of natural convection in inclined rectangular regions of differing aspect ratios, J. Heat Transfer 98 (1976) 67–71.

[8] S.M. Elshirbiny, G.D. Raithby, K.G.T. Hollands, Heat transfer by natural convection across vertical and inclined air layers, J. Heat Transfer 104 (1982) 96–102.

[9] S.M. Elshirbiny, K.G.T. Hollands, G.D. Raithby, Nusselt number distribution in vertical and inclined air layers, J. Heat Transfer 105 (1983) 406–408.

[10] H. Ozoe, H. Sayama, S.W. Churchill, Natural convection in an inclined rectangular channel at various aspect ratios and angles-experimental measurements, Int. J. Heat Mass Transfer 18 (1975) 1425–1431.

[11] H. Ozoe, H. Sayama, S.W. Churchill, Natural convection in an inclined square channel, Int. J. Heat Mass Transfer 17 (1974) 401–406.

[12] H. Ozoe, K. Yamamoto, H. Sayama, S.W. Churchill, Natural circulation in an inclined rectangular channel heated on one side and cooled in opposing side, Int. J. Heat Mass Transfer 17 (1974) 1209–1217.

[13] H. Ozoe, K. Fujii, N. Lior, S.W. Churchill, Long rolls generated by natural convection in an inclined rectangular enclosure, Int. J. Heat Mass Transfer 26 (1983) 1427–1438.

[14] Z.Y. Zhong, K.T. Yang, J.R. Lloyd, Variable property natural convection in titled cavities with thermal radiation, in: R.W. Lewis, V.T. Morgan (Eds.), Numerical Methods in Heat Transfer, vol. 3, Wiley, Chichester, 1985, pp. 195–214.

[15] R.A. Kuyper, T.H.H. Van Der Meer, C.J. Hoogendoorn, R.A.W.M. Henkes, Numerical study of laminar and turbulent natural convection in an inclined square cavity, Int. J. Heat Mass Transfer 36 (11) (1993) 2899–2911.

[16] R.A.W.M. Henkes, C.J. Hoogendoorn, Scaling of the laminar natural convection flow in an heated square cavity, Int. J. Heat Mass Transfer 36 (11) (1993) 2913–2925.

[17] J.A. Janssen, R.A.W.M. Henkes, C.J. Hoogendoorn, Transition to time-periodicity of a natural convection flow

in a 3D differentially heated cavity, Int. J. Heat Mass Transfer 36 (11) (1993) 2927–2940.
[18] Y.E. Karyakin, Transient natural convection in prismatic enclosures of arbitrary cross-section, Int. J. Mass Transfer 32 (1989) 1095–1103.
[19] T.S. Lee, Numerical experiment with fluid convection in titled nonrectangular enclosures, Numer. Heat transfer 19 (1991) 487–499.
[20] L.S. Yao, Natural convection along a vertical wavy surface, J. Heat Transfer 105 (1983) 465–468.
[21] L. Adjlout, O. Imine, A. Azzi, M. Belkadi, Numerical study of the natural convection in a cavity with undulated wall, in: Third International Thermal Energy and Environment Congress, Merrakech, Maroc, June 9–12, 1997.
[22] P.D. Thompson, F.C. Thames, F. Mastin, Automatic numerical generation of body-fitted curvilinear co-ordinate system, J. Comput. Phys. 15 (1974) 299–319.
[23] I. Catton, P.S. Ayyasme, R.M. Clever, Natural convection flow in a finite rectangular slot arbitrary oriented with respect to the gravity vector, Int. J. Heat Mass Transfer 17 (1974) 173–184.
[24] F.J. Hammady, J.R. Lloyd, H.Q. Yang, K.T. Yang, Study of local natural convection heat transfer in an inclined enclosure, Int. J. Heat Mass Transfer 32 (9) (1989) 1697–1708.